# Structure of Au(111) and Au(100) Single-Crystal Electrode Surfaces at Various Potentials in Sulfuric Acid Solution Determined by In Situ Surface X-ray Scattering

**Toshihiro Kondo,*,† Jun Morita,‡ Kazuya Hanaoka,‡ Satoru Takakusagi,‡ Kazuhisa Tamura,§ Masamitu Takahasi,§ Jun'ichiro Mizuki,§ and Kohei Uosaki*,‡**

*Department of Chemistry, Faculty of Science, Ochanomizu University, Ohtsuka, Bunkyo-ku, Tokyo 112-8610, Japan, Physical Chemistry Laboratory, Division of Chemistry, Graduate School of Science, Hokkaido University, Sapporo 060-0810, Japan, and Synchrotron Radiation Research Center, Japan Atomic Energy Agency, 1-1-1, Koto, Sayo-cho, Hyogo 679-5148, Japan*

*Received: April 3, 2007; In Final Form: July 3, 2007*

Potential-dependent surface structures of Au(111) and Au(100) single-crystal electrodes in a 50 mM $H_2SO_4$ solution were investigated at an atomic level using in situ surface X-ray scattering (SXS) techniques. It was confirmed that both the Au(111) and Au(100) surfaces were reconstructed with an attached submonolayer of an oxygen species, most probably water, at 0 V (vs Ag/AgCl). Results at +0.95 V supported a previously suggested model for both the Au(111) and the Au(100) electrodes that, based on infrared and scanning tunneling microscopy measurements, the surfaces were a $(1 \times 1)$ structure with the coadsorbed sulfate anion and hydronium cation ($H_3O^+$). At +1.05 V, where a small amount of an anodic current flowed, adsorption of a monolayer of oxygen species was observed on both surfaces. When the single-crystal gold electrodes were electrochemically oxidized at +1.40 V, the expansion of the gold surface by about one monolayer of Au atoms was observed, suggesting the penetration of oxygen into the surface gold layers (i.e., the formation of two layers of surface oxide). When the surface oxide was reduced at +0.65 V, the surface structure returned back to the structure observed at +0.95 V before the oxide formation (i.e., a $(1 \times 1)$ structure with coadsorbed sulfate anion and $H_3O^+$). When the potential was reduced to 0 V, the surfaces were reconstructed again but with slightly more random structures than those before the potential cycle.

## 1. Introduction

Gold is one of the most important materials for various applications, and the structure and properties of low index surfaces of single-crystal gold have been extensively studied not only in ultrahigh vacuum (UHV)[1−6] but also in electrochemical environments.[7−37] The surface structures of the single-crystal gold electrodes in electrolyte solutions have been investigated using various techniques, including conventional electrochemical methods,[7−15] scanning tunneling microscopy (STM),[16−28] and several optical techniques,[27−37] and were found to be strongly dependent on the potentials. It is well-known that the potential-induced reversible lifting and restoration of surface reconstruction (i.e., $(\sqrt{3} \times 23)$ for Au(111) and hexagonal closed-packing for Au(100) surfaces) take place around +0.35 V vs Ag/AgCl in a sulfuric acid solution.[18−24] STM investigation of these surfaces in atomic resolution showed that the phase transitions from reconstructed phase to $(1 \times 1)$ arrangement are accompanied with the adsorption of anions such as sulfate, chloride, bromide, and iodide, and when the potential is made more positive, the adsorbed anions form ordered phases.[7,8,11,20,21]

It has been suggested that when the potential is made further positive, oxidation takes place initially with the adsorption of $OH^-$ (reaction 1), followed by a turnover process, which leads to the formation of a two-atom thick oxide layer (reaction 2).[7−13]

$$Au + H_2O \rightarrow Au^{I}OH + H^+ + e^- \quad (1)$$

$$Au^{I}OH \rightarrow Au^{II}O + H^+ + e^- \quad (2)$$

Although the formation of Au−OH, Au−O, and $Au_2O_3$ species on the surface has been discussed based on the data of charge and capacitance obtained by conventional electrochemical techniques,[7−13] the electrochemical techniques cannot provide the structural information. The electrochemical quartz crystal microbalance (EQCM) technique was used to study the anion adsorption on the electrode surface,[14] but this only gives information of mass change on the electrode surface and cannot be applied for single-crystal electrodes. STM measurement provides structural information at atomic resolution but of the outermost layer only;[16−28] therefore, the surface structure of the electrode cannot be determined by STM when the surface is covered with adsorbates such as anions. Information obtained by optical techniques contains contributions not only from the electrode surface but also from the bulk.[27−37] Thus, the surface structures of the single-crystal gold electrodes at atomic resolution for wide potential regions, particularly in the oxide formation potential region, have not been clarified yet.

The surface X-ray scattering (SXS) technique is one of the best methods to investigate the three-dimensional (3D) interfacial structure at an atomic level.[27,28,38] Many in situ structural studies at electrode/electrolyte interfaces using the SXS technique have been carried out in the last 15 years.[39−52] For

* To whom correspondence should be addressed. E-mail: T.K.: kondo.toshihiro@ocha.ac.jp; K.U.: uosaki@pcl.sci.hokudai.ac.jp.
† Ochanomizu University.
‡ Hokkaido University.
§ Japan Atomic Energy Agency.

10.1021/jp072601j CCC: $37.00 
Published on Web 08/16/2007

example, we determined the structure of the underpotentially deposited (UPD) Ag layers on a Au(111)-(1 × 1) surface.[49] As far as the structure of gold electrodes is concerned, Ocko et al. investigated the structures of the reconstructed Au(111) and Au(100) surfaces in electrolyte solutions containing various halogen anions using in situ SXS.[39−42] There were, however, no structural analyses of gold single-crystal electrode/electrolyte interfaces in other potential regions using the in situ SXS technique.

In this paper, the potential-dependent structures of single-crystal Au(111) and Au(100) electrodes in sulfuric acid solution in wide potential regions (0 to +1.4 V) were investigated by X-ray reflectivity measurement, one of the SXS methods. Experimentally obtained reflectivity profiles of both Au(111) and Au(100) electrodes at all potentials were well fitted to the profiles, which were calculated using the following interfacial structural models.

## 2. Experimental

**2.1. Materials.** Au(111) and Au(100) single-crystal disks (diameter: 10 mm, thickness: 5 mm) were purchased from Surface Preparation Laboratory (The Netherlands). The disks were electrochemically etched in a solution containing 0.1 M $HClO_4$ and 5 mM NaCl[25] and then annealed at 850 °C for 10 h under an Ar atmosphere in an electric furnace (Denken, KDF S-70). Ultrapure reagent-grade $H_2SO_4$ and $HClO_4$ and reagent-grade NaCl were purchased from Wako Pure Chemicals and were used without further purification. Water was purified using a Milli-Q system (Yamato, WQ-500). Ultrapure $N_2$ (99.9995%) and Ar (99.999%) were purchased from Air−Water. A 6.0 $\mu$m thick Mylar film (Chemplex, D) was used as the window of a spectroelectrochemical cell, which was specially designed for the in situ SXS measurements and was made of Kel-F.[48]

**2.2. Electrochemical and In Situ SXS Measurements.** Both the cyclic voltammetry and the in situ SXS measurements were carried out using the spectroelectrochemical cell.[48] The electrode potential was controlled by a potentiostat/galvanostat (Hokuto Denko, HA-151), and an external potential was provided by a function generator (Hokuto Denko, HB-111). Cyclic voltammograms (CVs) were recorded on an X−Y recorder (Graphtech, WX1200). A Pt wire and Ag/AgCl electrode were used as counter and reference electrodes, respectively.

The spectroelectrochemical cell was set on a six-circle diffractometer (HUBER, 5020) installed in a bending-magnet beamline BL4C at Photon Factory or on a $\kappa$-type diffractometer (Newport) installed in a bending-magnet beamline BL14B1 at SPring-8. X-ray radiation was monochromated by a Si(111) double-crystal system and was focused by a Rh-coated bending mirror. The beam size of the incident X-ray was 0.2 mm (vertical) × 0.2−0.5 mm (horizontal), which was adjusted by a slit placed in front of the cell. Intensity of the incident X-ray was measured by the ion chamber, which was placed in front of the sample, in order to normalize the data with the incident X-ray intensity. A wavelength of 1.100 Å was selected to avoid any fluorescence from the Au substrate. In the SXS measurements, a hexagonal coordinate system in which H and K are parallel to the surface and L is normal to the surface was used. H, K, and L have units of $a^*$, $b^*$, and $c^*$, respectively, which are defined as $|a^*| = |b^*| = 4\pi/\sqrt{3}a = 2.52$ Å$^{-1}$ and $|c^*| = 2\pi/\sqrt{6}a = 0.89$ Å$^{-1}$, where $a$ is the nearest neighbor distance, 2.885 Å. Reflectivity measurements were carried out along the (00L) direction, that is, normal to the surface, and each reflectivity was a rocking-curve integrated intensity, which was normalized with the incident X-ray intensity.[46]

**2.3. Procedures.** Prior to each measurement, the Au(111) and Au(100) disks were flame annealed using a Bunsen burner or a hydrogen flame and were slowly cooled in air. It was then transferred to the spectroelectrochemical cell with a drop of pure water on the surface to avoid any surface contamination. Measurements were carried out in a 50 mM $H_2SO_4$ electrolyte solution, which was deaerated by passing the ultrapure $N_2$ gas through the solution for more than 30 min before it was injected to the cell. The electrode made contact with the electrolyte solution while keeping the potential at 0 V (vs Ag/AgCl), where the electrode surfaces were reconstructed. Only the (111) or (100) face was in contact with the electrolyte solution during the electrochemical measurements. Electrode potential was scanned for the positive direction from 0 V and was stopped at a certain potential, where the SXS measurement was going to be carried out, while keeping the thickness of the solution layer between the electrode and Mylar window at ca. 5 mm (thick electrolyte configuration). After that, the electrode surface was pushed to the Mylar window (thin electrolyte configuration) so that the X-ray scattering by the solution was kept at a minimum and no further electrochemical reaction proceeded. The thickness of the electrolyte layer between the electrode and the window in this configuration was estimated to be ca. 30 $\mu$m. The cell was turned over and then the in situ SXS measurement was carried out.[48]

**2.4. Data Analysis.** In the reflectivity curves, several peaks of the scattering intensity near $L = 0$, 3, and 6 ($H = K = 0$) for Au(111) and near $L = 0$, 2, and 4 for Au(100) were observed. The peaks around $L = 3$ and 6 for Au(111) correspond to the cubic (1,1,1) and (2,2,2), respectively, and those around $L = 2$, and 4 for Au(100) correspond to the cubic (1,0,0) and (2,0,0), respectively. Between these peaks, the reflectivity was low and depended on the detailed structure of the interface. Structures along the direction normal to the electrode surface were quantitatively determined from the least-square fitting to the reflectivity data with a kinematical calculation based on a specific interfacial model.[39,46,53,54] All the fittings were carried out using models of three layers on top of the Au substrate. The amounts of various atoms in each layer were estimated by considering that one monolayer (ML) corresponds to 1.39 × $10^{15}$ and 1.20 × $10^{15}$ atoms cm$^{-2}$ on Au(111) and Au(100), respectively. In the fitting, a three-layer structure model, where each layer consists of gold, oxygen, or sulfer, was assumed. Fittings with all possible structure models were carried out, and a fitting result, which gave the least value of $\chi^2$ among all the fitting results, was taken as a best-fitted result.

For the gold oxide layers, the contribution of oxygen was neglected, because the electron density of the oxygen atom is only 10% of that of the gold atom.

## 3. Results and Discussions

**3.1. Au(111) Electrode.** Figure 1 shows a CV of a Au(111) single-crystal electrode in a 50 mM $H_2SO_4$ electrolyte solution obtained under the thick electrolyte configuration. Sharp anodic and cathodic peaks were observed at +1.30 V and +0.91 V, respectively. The former peak can be assigned to the oxide formation and the latter to the reduction of oxide. Inset of Figure 1 shows a CV in the narrower potential range (0 through +1.00 V) with a magnified current scale. A pronounced anodic peak at +0.31 V due to ($\sqrt{3}$ × 23) → (1 × 1) structural transition and a couple of spikes due to an order (at +0.86 V)/disorder (at +0.84 V) transition of adsorbed sulfate anions were observed. Almost no current flowed at potentials more positive than the potential of the order transition peak up to 1.05 V, and

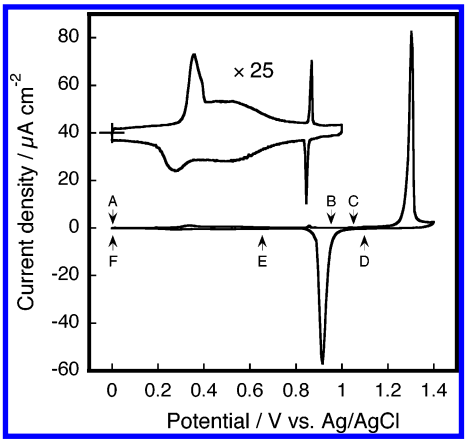


**Figure 1.** A CV at the Au(111) electrode measured in a 50 mM $H_2SO_4$ electrolyte solution with a scan rate of 20 mV $s^{-1}$. Inset: A CV with an expanded current scale in the potential range of 0 through +1.00 V and measured with a scan rate of 5 mV $s^{-1}$. Arrows A−F represent the potentials where SXS measurements were carried out.

only a very small anodic current was observed at potentials more positive than +1.05 V before the oxide formation. These features were exactly the same as those of high quality Au(111) electrodes,[18,20,23,24] indicating that the quality of the Au(111) surface used in the present study was very high.

SXS measurements were carried out at potentials indicated by arrows A−F in Figure 1, and the reflectivity profiles measured at these potentials are shown in Figure 2. Values of standard errors of the scattered X-ray intensity were shown as error bars in the figure. The structure parameters obtained from the least-square fitting with a kinematical calculation at various potentials are listed in Table 1. On the basis of these values obtained from a fitting, the structures along the direction normal to the surface at the Au(111) electrode/$H_2SO_4$ electrolyte solution interface were determined as described below.

*A. At 0 V Before Potential Scan.* Best-fit data showed that the interfacial structure at this potential is the Au(111)-($\sqrt{3} \times 23$) reconstructed surface covered with 0.74 ML of oxygen species[55] as schematically illustrated in Figure 3A, and the distance between the oxygen species and the topmost Au layer was 2.31 Å (Table 1). The present results are in good agreement with those suggested by Ocko et al. from the X-ray reflectivity data for a Au(111) electrode in a 0.1 M $HClO_4$ solution containing various halogen anions, where the Au(111) surface was reconstructed in a relatively negative potential region with the Au(111)-($\sqrt{3} \times 23$) structure covered with a double layer of water molecules, with the coverage of 0.7 and 0.3 ML for the first and second layers, respectively, and the distance between the first water layer and the topmost Au layer was 2.9 Å.[39−41]

*B. At +0.95 V.* Figure 2B shows the reflectivity profiles measured at +0.95 V, which was more positive than the potential of the current spike (Figure 1). Best-fit data showed that at this potential the reconstruction was lifted, and the Au-(111)-(1 × 1) substrate was covered, with the first, second, and third layers composed of 0.88 ML of oxygen, 0.22 ML of sulfur, and 0.24 ML of oxygen species,[55] respectively, as schematically illustrated in Figure 3B. The distances between the outermost Au layer and the first, the first and the second, and the second and the third layers were 2.37, 1.08, and 1.86 Å, respectively (Table 1). These numbers are in good agreement with those estimated from a model proposed by Kolb et al., based on STM,[20] and by Ataka and Osawa, based on IR.[56] They suggested that the sulfate anion ($SO_4^{2-}$ or $HSO_4^-$) and hydronium ion ($H_3O^+$) were coadsorbed on the Au(111)-(1 × 1) surface with a ($\sqrt{3}\times\sqrt{7}$)*R*19.1° structure with a molar ratio of 1:1 through three oxygen atoms and three hydrogen atoms, respectively.

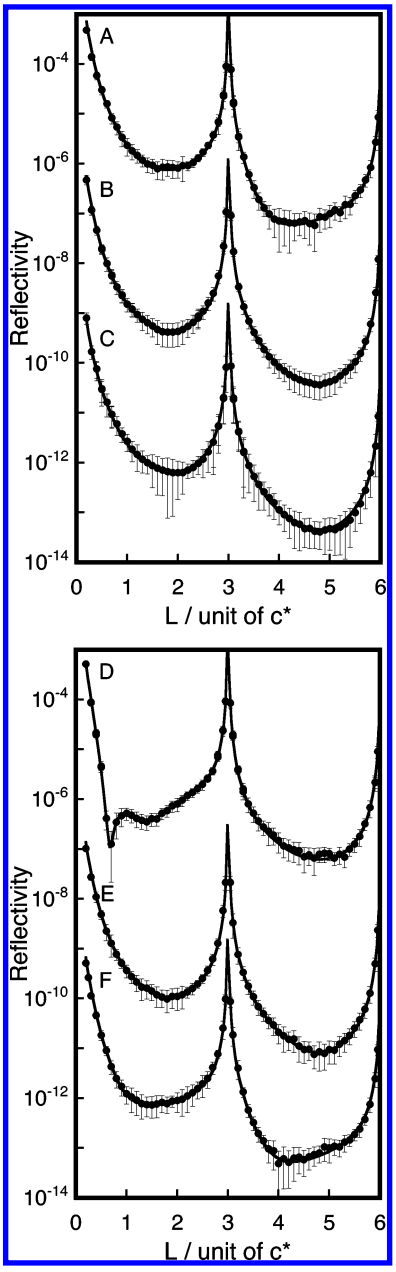


**Figure 2.** The reflectivity profiles of the Au(111)/50 mM $H_2SO_4$ solution interface (A) at 0 V just after dipping the electrode, (B) at +0.95 V (÷ 1000), (C) at +1.05 V (÷ 1000000), (D) at +1.40 V, (E) at +0.65 V (÷ 1000), and (F) at 0 V after potential cycling (÷ 1000000). The open circles and the solid lines are, respectively, the experimental data and the calculated curves fitted by the least-squares method with a kinematical calculation using models with three layers on the Au(111) substrate as schematically shown in Figure 3. Values of standard errors of the scattered X-ray intensity were shown as error bars in the figure.

Relatively large root mean square (rms) values of these layers (Table 1) reflect the relatively rough surface of the Au(111)-(1 × 1) as a result of a lifting of the ($\sqrt{3} \times 23$) reconstructed structure.

*C. At +1.05 V.* Figure 2C shows the reflectivity profiles measured at +1.05 V, where very small anodic current flowed (Figure 1). Best-fit data showed that the Au(111)-(1 × 1) substrate was covered with the first, the second, and the third layers composed of 1.00 ML of gold, 0.040 ML of gold, and 1.00 ML of oxygen species,[55] respectively, as schematically illustrated in Figure 3C. The distance between the second layer

**TABLE 1: Structural Parameters Obtained from the Analyses of the Specular Rod Profiles at Au(111) Electrode/electrolyte Interface at Various Potential Regions as a Three-layers Model on Au(111)[a]**

| | 0 V (before potential cycle) | +0.95 V | +1.05 V | +1.40 V | +0.65 V | 0 V (after potential cycle) |
|---|---|---|---|---|---|---|
| $f_{m1}$ | $f_{Au}$ | $f_O$ | $f_{Au}$ | $f_{Au}$ | $f_O$ | $f_{Au}$ |
| $f_{m2}$ | $f_{Au}$ | $f_S$ | $f_{Au}$ | $f_{Au}$ | $f_S$ | $f_{Au}$ |
| $f_{m3}$ | $f_O$ | $f_O$ | $f_O$ | $f_O$ | $f_O$ | $f_O$ |
| distance, $z_{ms1}$/Å | 2.36 ± 0.01 | 2.37 ± 0.02 | 2.36 ± 0.02 | 2.99 ± 0.03 | 2.36 ± 0.03 | 2.43 ± 0.03 |
| distance, $z_{m12}$/Å | 2.43 ± 0.01 | 1.08 ± 0.03 | 2.36 ± 0.01 | 2.50 ± 0.05 | 1.07 ± 0.04 | 2.90 ± 0.02 |
| distance, $z_{m23}$/Å | 2.31 ± 0.02 | 1.86 ± 0.03 | −0.08 ± 0.01 | 1.55 ± 0.04 | 1.86 ± 0.03 | 0.43 ± 0.03 |
| coverage, $\rho_{m1}$/ML | 1.00 ± 0.01 | 0.88 ± 0.02 | 1.00 ± 0.02 | 0.73 ± 0.02 | 0.87 ± 0.02 | 1.00 ± 0.02 |
| coverage, $\rho_{m2}$/ML | 1.04 ± 0.01 | 0.22 ± 0.02 | 0.04 ± 0.01 | 0.31 ± 0.01 | 0.22 ± 0.02 | 1.06 ± 0.03 |
| coverage, $\rho_{m3}$/ML | 0.74 ± 0.02 | 0.24 ± 0.01 | 1.00 ± 0.01 | 1.00 ± 0.01 | 0.24 ± 0.02 | 0.99 ± 0.02 |
| RMS, $\sigma_{m1}$/Å | 0.09 ± 0.01 | 0.26 ± 0.02 | 0.09 ± 0.01 | 0.63 ± 0.03 | 0.14 ± 0.02 | 0.09 ± 0.04 |
| RMS, $\sigma_{m2}$/Å | 0.13 ± 0.01 | 0.50 ± 0.03 | 0.13 ± 0.03 | 0.67 ± 0.04 | 0.13 ± 0.02 | 0.73 ± 0.03 |
| RMS, $\sigma_{m3}$/Å | 0.37 ± 0.02 | 0.36 ± 0.03 | 0.99 ± 0.05 | 1.11 ± 0.03 | 0.43 ± 0.03 | 0.39 ± 0.03 |

[a] The atomic form factors, $f_{Au}$, $f_O$, and $f_S$ are of Au, O, and S, respectively. The term $f_m$ means the atomic form factor of specie of m. The subscripts of m1, m2, and m3 represent first layer, second layer, and third layer, respectively. Distances of $z_{ms1}$, $z_{m12}$, and $z_{m23}$ represent atomic layer distances between the outermost substrate and first layers, between first and second layers, and between second and third layers, respectively.

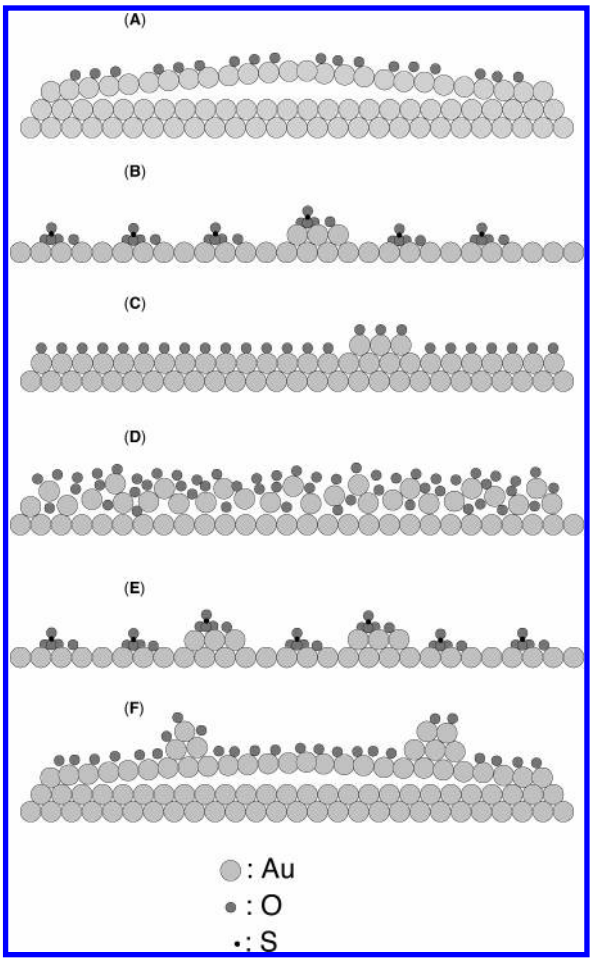


**Figure 3.** The schematic illustrations of the Au(111) electrode/$H_2SO_4$ solution interface at various potentials. Hydrogen atoms are not shown because their positions cannot be determined by SXS measurements.[55]

of Au and the third layer of the oxygen species was negative (Table 1), indicating that the gold surface was expanded. This result indicated that the adsorbed sulfate anion at +0.95 V was desorbed and oxygen species were adsorbed onto the Au(111)-(1 × 1) surface. The height of the oxygen species layer calculated from the present data was ca. 2.3 Å. This value was slightly different from the value (1.5 Å) obtained by STM[18] but closely matched the calculated value (2.14 Å) when the oxygen atom was adsorbed at the atop site of the Au substrate. Because STM data did not show the real geometric height but contained electronic information, the geometric height obtained by SXS measurements should be more accurate. Although there have been many discussions on the nature of the adsorbed oxygen species (i.e., O, OH, $OH^-$, water molecules, $H_3O^+$, etc.) in this potential region,[8−12,26,56] one cannot distinguish these species based on the results of SXS measurements because X-ray is not scattered by hydrogen atoms, but it can be concluded that oxygen species were adsorbed at the atop site of the underlying Au(111)-(1 × 1) surface.[55]

*D. At +1.40 V.* The X-ray scattering intensity gradually changed with time, indicating that the surface reaction (i.e., oxide formation reaction) took place even in the thin electrolyte configuration, although only a very small current flowed. Because it requires a very long time (10−12 h) to obtain one reflectivity curve, the SXS measurement was carried out not at +1.40 V but at +1.10 V. The positive-going potential scan was reversed at +1.40 V and was scanned negatively with a scan rate of 20 mV $s^{-1}$. As soon as the potential became +1.10 V, the potential scan was stopped, the electrode surface was pushed to the Mylar window, and the reflectivity measurement was started. Data obtained at this potential was considered to be the one at +1.40 V because neither anodic nor cathodic current was observed in the negative-going potential scan between +1.40 V and +1.10 V and because the X-ray scattering intensity did not change at this potential.

Figure 2D shows the reflectivity profiles measured at +1.10 V. Best-fit data showed that the Au(111)-(1 × 1) substrate was covered with the first, the second, and the third layers composed of 0.73 ML of gold, 0.31 ML of gold, and 1.00 ML of oxygen species,[55] respectively. The results indicating that the coverage of gold atoms in the first and the second layers was less than 1 ML showed that gold atoms coexisted with oxygen atoms, indicating that gold oxide was formed, although we cannot determine the fraction of oxygen atoms in these oxide layers. The schematic illustration of the interfacial structure is shown in Figure 3D. As a result of the penetration of oxygen atoms into the gold surface layers, the distances between the outermost layer of the gold substrate and the first layers and between the first and the second layers were 2.90 and 2.50 Å, respectively, and were larger than the value (2.36 Å) of the bulk Au(111).

The above result supports the model proposed by Conway et al. based on the results of conventional electrochemical measurements that the two-atom thick oxide layer was formed as a result of a turnover reaction.[7,8] The total number of gold atoms in these oxide layers was equivalent to 1.04 ML, which was

exactly the same as that of the gold coverage of the reconstructed Au(111)-($\sqrt{3} \times 23$) surface observed at 0 V. This indicates that only the gold atoms in the outermost layer are electrochemically oxidized in the potential cycle up to +1.40 V vs Ag/AgCl. This result also confirms that the real surface area can be calculated from the charge of the current peak of the oxide reduction.[13]

*E. At +0.65 V.* Figure 2E shows the reflectivity profiles measured at +0.65 V, which is more negative than that of the oxide reduction peak (Figure 1), after the positive-going potential scan to +1.40 V. Best-fit data showed that the first, the second, and the third layers on the Au(111)-(1 × 1) substrate were composed of 0.87 ML of oxygen species, 0.22 ML of sulfur, and 0.24 ML of oxygen species, respectively. These values closely matched those obtained at +0.95 V in the positive going scan (Section *B*). Furthermore, the distances between the substrate and the first layer, the first layer and the second layer, and the second layer and the third layer (Table 1) were all in good agreement with those obtained at +0.95 V before the oxide formation. Thus, the interfacial structure at this potential is same as that obtained at +0.95 V in the positive going scan (section B), indicating that the sulfate and $H_3O^+$ were coadsorbed with a ($\sqrt{3}\times\sqrt{7}$)R19.9° structure through three oxygen atoms and three hydrogen atoms, respectively, which is schematically shown in Figure 3E. One must note, however, that the lateral order of the adsorbates cannot be confirmed based only on the reflectivity data.

*F. At 0 V.* Figure 2F shows the reflectivity profile measured at 0 V after a potential cycle. Best-fit data showed that the Au(111)-($\sqrt{3} \times 23$) reconstructed surface was covered with 0.99 ML of oxygen species, as was observed at 0 V before the potential cycle; the first, the second, and the third layers were composed of gold, gold, and oxygen species, respectively. The schematic illustration of the interfacial structure is shown in Figure 3F. The comparison of the structural parameters measured at 0 V before and after the potential cycle showed that the distances between outermost substrate and first layers and first and second layers, coverage of O and Au atoms in the outermost two layers, and rms values of the all three layers, became slightly larger after the potential cycle. These results indicate that small Au clusters existed on the reconstructed Au(111)-($\sqrt{3} \times 23$) surface (i.e., the surface was roughened). This is in good agreement with the well-known fact that once the gold electrode surface is oxidized, oxygen atoms penetrate into the outermost gold layer and the electrode surface is roughened even after the complete reduction of the surface oxide.[17,22,52]

**3.2. Au(100) Electrode.** Figure 4 shows a CV of a Au(100) single-crystal electrode in a 50 mM $H_2SO_4$ electrolyte solution obtained under the thick electrolyte configuration. Sharp anodic and cathodic peaks were observed at +1.11 V and +0.93 V, respectively. The former peak can be assigned to the oxide formation and the latter to the reduction of oxide. Another small anodic current was also observed around +1.05 V. The inset of Figure 4 shows a CV in the narrower potential range (0 through +1.00 V) with a magnified current scale. A pronounced anodic peak due to a hexagonal closed-packing → (1 × 1) structural transition was observed at +0.39 V. These features were exactly the same as those of high quality Au(100),[19−23] indicating that the quality of the Au(100) surface used in the present study was very high. SXS measurements were carried out at the potentials indicated by arrows **A**−**F** in Figure 4.

Figures 5 shows the reflectivity profiles measured at various potentials shown in Figure 4. Values of standard errors of the scattered X-ray intensity were shown as error bars in the figure. The structure parameters obtained from the least-square fitting with a kinematical calculation at various potentials are listed in Table 2. On the basis of these values obtained from a fitting, the structures along the direction normal to the surface at an Au(100) electrode/$H_2SO_4$ electrolyte solution interface were determined as below.

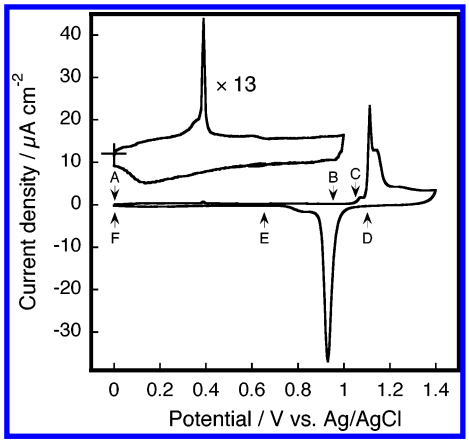


**Figure 4.** A CV at the Au(100) electrode measured in a 50 mM $H_2SO_4$ electrolyte solution with a scan rate of 20 mV $s^{-1}$. Inset: A CV with an expanded current scale in the potential range of 0 through +1.00 V and measured with a scan rate of 5 mV $s^{-1}$. Arrows A−F represent the potentials where SXS measurements were carried out.

*A. At 0 V Before Potential Scan.* Best-fit data showed that the reconstructed hexagonal closed-packed Au(100) surface was covered with 1.02 ML of oxygen species,[55] as schematically illustrated in Figure 6**A**. The distance between the second (gold) and the third (oxygen species) layers (1.98 Å) was shorter, the coverage of the third layer (oxygen species) of 1.02 ML was higher, and the rms value of the second layer (outermost gold layer) of 0.52 was larger than those in the case of Au(111). These values suggest the presence of several Au clusters with oxygen species on the reconstructed surface and indicate that the surface flatness of reconstructed Au(100), even just after annealing and quenching, is slightly less than that of reconstructed Au(111).

*B. At + 0.95 V.* Figure 5B shows the reflectivity profiles measured at +0.95 V. Best-fit data showed that the first, the second, and the third layers on the Au(100)-(1 × 1) substrate were composed of 0.61 ML of oxygen species,[55] 0.20 ML of sulfur, and 0.41 ML of oxygen species, respectively. Distances between the outermost layer of the substrate and the first layer, the first and the second layers, and the second and third layers were 1.98, 0.99, and 1.00 Å, respectively. The schematic illustration of the interfacial structure is shown in Figure 6B. These numbers are in good agreement with those obtained from a model proposed by Kolb et al. based on the STM results.[20,21] They suggested that the sulfate anion and $H_3O^+$ were coadsorbed onto the Au(100)-(1 × 1) surface with a (1.4 × 3.6) structure with a molar ratio of 1:1 through two oxygen atoms and three hydrogen atoms, respectively. Relatively large rms values of these layers are due to the relatively rough surface of the Au-(100)-(1 × 1) as a result of a lifting of the reconstructed hexagonal closed-packed structure.

*C. At +1.05 V.* Figure 5C shows the reflectivity profiles measured at +1.05 V, around which only a very small anodic current flowed (Figure 4). Best-fit data showed that the first, the second, and the third layers on the Au(100)-(1 × 1) substrate were composed of 1.00 ML of gold, 0.16 ML of gold, and 1.01 ML of oxygen species,[55] respectively. The schematic illustration of the interfacial structure is shown in Figure 6**C**. The distance between the second (gold) and the third (oxygen

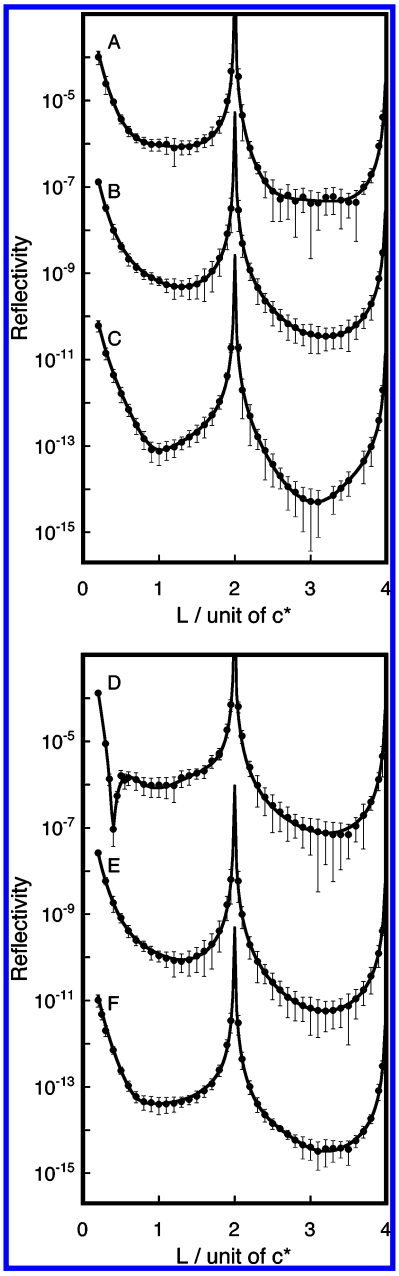


**Figure 5.** The specular rod profiles of the Au(100)/50 mM $H_2SO_4$ solution interface (A) at 0 V just after dipping the electrode, (B) at +0.95 V (÷ 1000), (C) at +1.05 V (÷ 1000000), (D) at +1.40 V, (E) at +0.65 V (÷ 1000), and (F) at 0 V after potential cycling (÷ 1000000). The open circles and the solid lines are, respectively, the experimental data and the calculated curves fitted by the least-squares method with a kinematical calculation using models with three layers on the Au(100) substrate as schematically shown in Figure 6. Values of standard errors of the scattered X-ray intensity were shown as error bars in the figure.

species) layers was 0.26 Å, which was very small, indicating that the gold surface was expanded. This result indicated that the adsorbed sulfate anion at +0.95 V was desorbed, and oxygen species were adsorbed on the Au(100)-(1 × 1) surface. The height of the layer of oxygen species calculated from the present data was ca. 2.3 Å, showing that the oxygen species were adsorbed at the atop site of the underlying Au(100)-(1 × 1) surface.

*D. At +1.40 V.* As observed at the Au(111) electrode, when the potential was kept at +1.40 V, X-ray scattering intensity from the Au(100)/electrolyte solution interface changed with time, even in the thin electrolyte configuration. Thus, the SXS measurement was carried out not at +1.40 V but at +1.10 V. The positive-going potential scan was reversed at +1.40 V and was scanned negatively with a scan rate of 20 mV $s^{-1}$. As soon as the potential became +1.10 V, the potential scan was stopped, the electrode surface was pushed to the Mylar window, and reflectivity measurement was started. Data obtained at this potential was considered to be the one at +1.40 V as was the case at the Au(111) electrode.

Figure 5D shows the reflectivity profiles measured at +1.10 V. Best-fit data showed that the first, the second, and the third layers on the Au(100)-(1 × 1) substrate were composed of 0.73 ML of gold, 0.43 ML of gold, and 1.01 ML of oxygen species,[55] respectively. As was case at the Au(111) electrode, the first and the second layers should consist of Au oxide, as a result of a turnover reaction. The schematic illustration of the interfacial structure at this potential is shown in Figure 6D.

The total number of gold atoms in these oxide layers was 1.16 ML, which was exactly the same as that of the coverage of the reconstructed Au(100) surface observed at 0 V. This result indicates that only the gold atoms in the outermost layer are electrochemically oxidized in the potential cycle up to +1.40 V, confirming that we can calculate the real surface area of Au(100) from the charge of the oxide reduction peak as in the case for the Au(111) electrode.

*E. At +0.65 V.* Figure 5E shows the reflectivity profiles measured at +0.65 V, which is more negative than that of the oxide reduction peak in Figure 4. Best-fit data showed that the first, the second, and the third layers on the Au(100)-(1 × 1) substrate were composed of 0.61 ML of oxygen species,[55] 0.22 ML of sulfur, and 0.41 ML of oxygen species, respectively. This result closely matched that obtained at +0.95 V in the positive-going scan. Furthermore, the distances between the substrate and the first layer, the first layer and the second layer, and the second layer and the third layer (Table 2) were all in good agreement with those obtained at +0.95 V before the oxide formation. Thus, the interfacial structure at this potential is same as that obtained at +0.95 V in the positive-going scan (Section B), indicating that the sulfate and $H_3O^+$ were coadsorbed with a (1.4 × 3.6) structure through two oxygen atoms and three hydrogen atoms, respectively, as schematically illustrated in Figure 6E. One must note, however, that lateral order of the adsorbates cannot be confirmed based only on the reflectivity data.

*F. At 0 V.* Figure 5F shows the reflectivity profile measured at 0 V after a potential cycle. Best-fit data showed that the Au-(100)-hexagonal closed-packing reconstructed surface was covered with 0.99 ML of oxygen species,[55] as well as that measured at 0 V before the potential cycle; the first, the second, and the third layers on the Au(100)-(1 × 1) substrate were composed of gold, gold, and oxygen species, respectively. The schematic illustration of the interfacial structure is shown in Figure 6F. The comparison of the structural parameters measured at 0 V before and after the potential cycle showed that the distances between the first and second layers and between the second and third layers, coverage of O and Au atoms in the outermost two layers, and rms values of the all three layers became slightly larger after the potential cycle. These results indicate that small Au clusters existed on the reconstructed hexagonal closed-packed Au(100) surface (i.e., the surface was roughened). This is in good agreement with the well-known fact that once the gold electrode surface is oxidized, oxygen atoms penetrate into the outermost gold layer, and the electrode surface is roughened even after the complete reduction of the surface oxide.[22,52] The degree of the roughening on Au(100)

**TABLE 2: Structural Parameters Obtained from the Analyses of the Specular Rod Profiles at Au(100) Electrode/electrolyte Interface at Various Potential Regions as a Three-layers Model on Au(100)[a]**

| | 0 V (before potential cycle) | +0.95 V | +1.05 V | +1.40 V | +0.65 V | 0 V (after potential cycle) |
|---|---|---|---|---|---|---|
| $f_{m1}$ | $f_{Au}$ | $f_O$ | $f_{Au}$ | $f_{Au}$ | $f_O$ | $f_{Au}$ |
| $f_{m2}$ | $f_{Au}$ | $f_S$ | $f_{Au}$ | $f_{Au}$ | $f_S$ | $f_{Au}$ |
| $f_{m3}$ | $f_O$ | $f_O$ | $f_O$ | $f_O$ | $f_O$ | $f_O$ |
| distance, $z_{ms1}$/Å | 2.04 ± 0.01 | 1.98 ± 0.03 | 2.04 ± 0.03 | 2.65 ± 0.04 | 1.99 ± 0.04 | 2.04 ± 0.02 |
| distance, $z_{m12}$/Å | 2.45 ± 0.01 | 0.99 ± 0.03 | 2.04 ± 0.02 | 2.18 ± 0.03 | 0.99 ± 0.04 | 2.49 ± 0.03 |
| distance, $z_{m23}$/Å | 1.98 ± 0.01 | 1.00 ± 0.03 | 0.26 ± 0.02 | 1.85 ± 0.04 | 1.00 ± 0.05 | 2.00 ± 0.03 |
| coverage, $\rho_{m1}$/ML | 1.00 ± 0.02 | 0.61 ± 0.02 | 1.00 ± 0.02 | 0.73 ± 0.03 | 0.61 ± 0.02 | 1.00 ± 0.03 |
| coverage, $\rho_{m2}$/ML | 1.16 ± 0.03 | 0.20 ± 0.03 | 0.16 ± 0.02 | 0.43 ± 0.03 | 0.22 ± 0.04 | 1.23 ± 0.02 |
| coverage, $\rho_{m3}$/ML | 1.02 ± 0.02 | 0.41 ± 0.02 | 1.01 ± 0.02 | 1.01 ± 0.03 | 0.41 ± 0.03 | 0.99 ± 0.03 |
| RMS, $\sigma_{m1}$/Å | 0.09 ± 0.02 | 0.24 ± 0.03 | 0.16 ± 0.03 | 0.62 ± 0.03 | 0.15 ± 0.03 | 0.15 ± 0.02 |
| RMS, $\sigma_{m2}$/Å | 0.52 ± 0.02 | 0.51 ± 0.03 | 0.32 ± 0.03 | 0.84 ± 0.03 | 0.45 ± 0.05 | 0.95 ± 0.03 |
| RMS, $\sigma_{m3}$/Å | 0.27 ± 0.01 | 0.87 ± 0.04 | 0.15 ± 0.02 | 1.12 ± 0.04 | 0.69 ± 0.05 | 0.96 ± 0.03 |

[a] The atomic form factors, $f_{Au}$, $f_O$, and $f_S$ are of Au, O, and S, respectively. The term $f_m$ means the atomic form factor of specie of m. The subscripts of m1, m2, and m3 represent first layer, second layer, and third layer, respectively. Distance of $z_{ms1}$, $z_{m12}$, and $z_{m23}$ represent atomic layer distances between the outermost substrate and first layers, between first and second layers, and between second and third layers, respectively.

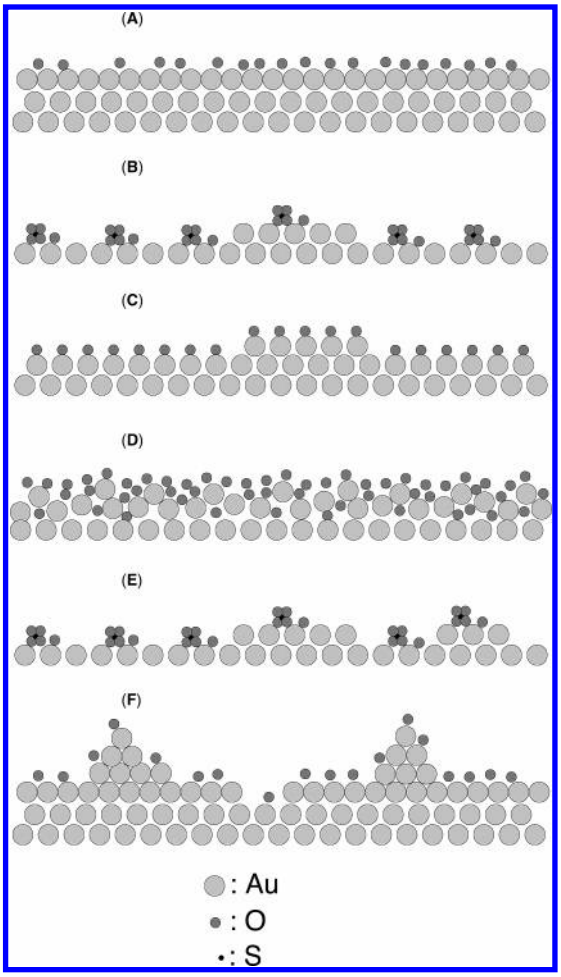


**Figure 6.** The schematic illustrations of the Au(100) electrode/$H_2SO_4$ solution interface at various potentials. Hydrogen atoms are not shown because their positions cannot be determined by SXS measurements.[55]

was much higher than that on Au(111), possibly because the oxygen atoms can more easily penetrate into the Au surface layer during the oxide formation for the square-arranged Au(100)-(1 × 1) surface than for the hexagonal closed-packed Au(111)-(1 × 1) surface.

## 4. Conclusion

The potential dependent structures of single-crystalline Au(111) and Au(100) electrodes were investigated in a sulfuric acid solution in wide potential regions (0 through +1.4 V) at an atomic level using an in situ SXS technique. At all potentials, the obtained reflectivity profiles were well-fitted using schematic three-layer models for the interfacial structure along the direction normal to the surface. It was confirmed that both Au(111) and Au(100) surfaces were reconstructed with an attached submonolayer of oxygen species at 0 V, the reconstruction was lifted, and the sulfate anion and $H_3O^+$ were coadsorbed at both electrodes at +0.95 V, as previously reported for both electrodes.[20−24,39−42] At +1.05 V, where a very small anodic current flowed, adsorption of a monolayer of oxygen species at the atop site of both the Au(111)-(1 × 1) and Au(100)-(1 × 1) surfaces was suggested. When the single-crystalline gold electrodes were electrochemically oxidized at +1.40 V, the gold surface was expanded by ca. one monolayer of Au atoms. The formation of two layers of surface oxide as a result of a penetration of oxygen into the surface gold layer was suggested. When the surface oxide was reduced at +0.65 V, the surface structure returned back to the (1 × 1) structure with coadsorbed sulfate anion and $H_3O^+$. When the potential was reduced to 0 V, both surfaces were reconstructed again but with slightly more random atomic arrangement than before the potential cycle.

**Acknowledgment.** This work was partially supported by Grants-in-Aid for Scientific Research (KAKENHI) in Priority Area of "Molecular Nano Dynamics" (Nos. 16072202 and 17034017) from the Ministry of Education, Culture, Sports, Science, and Technology. The synchrotron radiation experiments were performed as projects approved by the Photon Factory Program Advisory Committee (PAC Nos. 2002G059 and 2003G028) and by the Japan Synchrotron Radiation Research Institute (JASRI) (proposal Nos. 2002B0225 and 2003A0702).

## References and Notes

(1) Fedak, D. G.; Gjostein, N. A. *Surf. Sci.* **1967**, *8*, 77−97.
(2) Van Hove, M. A.; Koestner, R. J.; Stair, P. C.; Biberian, J. P.; Kesmodel, L. L.; Bartos, I.; Somorjai, G. A. *Surf. Sci.* **1981**, *103*, 189−217.
(3) Tanishiro, Y.; Kanamori, H.; Takayanagi, K.; Yagi, K.; Honjo, G. *Surf. Sci.* **1981**, *111*, 395−413.
(4) Binnig, G. K.; Rohrer, H.; Gerber, C.; Stoll, E. *Surf. Sci.* **1984**, *144*, 321−335.
(5) Harten, U.; Lahee, A. M.; Toennies, J. P.; Woell, C. *Phys. Rev. Lett.* **1985**, *54*, 2619−2622.
(6) Barth, J. V.; Brune, H.; Ertl, G.; Behm, R. J. *Phys. Rev. B* **1990**, *42*, 9307−9318.
(7) Angerstein-Kozlowska, A.; Conway, B. E.; Hamelin, A.; Stoicoviciu, L. *Electrochim. Acta* **1986**, *31*, 1051−1061.

(8) Angerstein-Kozlowska, A.; Conway, B. E.; Hamelin, A.; Stoicoviciu, L. *J. Electroanal. Chem.* **1987**, *228*, 429−453.
(9) Bourkane, S.; Gabrielle, C.; Huet, F.; Keddam, M. *Electrochim. Acta* **1993**, *38*, 1023−1028.
(10) Bourkane, S.; Gabrielli, C.; Keddam, M. *Electrochim. Acta* **1993**, *38*, 1827−1835.
(11) Conway, B. E. *Prog. Surf. Sci.* **1995**, *49*, 331−452.
(12) Dickertmann, D.; Schultz, J. W.; Vetter, K. *J. Electroanal. Chem.* **1974**, *55*, 429−443.
(13) Woods, R. In *Electroanalytical Chemistry: A Series of Advances*; Bard, A. J. Ed.; Marcel Dekker: New York, 1988; p 1.
(14) Lei, H.-W.; Uchida, H.; Watanabe, M. *Langmuir* **1997**, *13*, 3523−3528.
(15) Ye, S.; Ishibashi, C.; Shimazu, K.; Uosaki, K. *J. Electrochem. Soc.* **1998**, *145*, 1614−1623.
(16) Schneeweiss, M. A.; Kolb, D. M. *Solid State Ionics* **1997**, *94*, 171−179.
(17) Vitus, C. M.; Davenport, A. J. *J. Electrochem. Soc.* **1994**, *141*, 1291−1298.
(18) Honbo, H.; Sugawara, S.; Itaya, K. *Anal. Chem.* **1990**, *62*, 2424−2429.
(19) Honbo, H.; Itaya, K. *J. Chim. Phys.* **1991**, *88*, 1477−1489.
(20) Cuesta, A.; Kleinert, M.; Kolb, D. M. *Phys. Chem. Chem. Phys.* **2000**, *2*, 5684−5690.
(21) Kleinert, M.; Cuesta, A.; Kibler, L. A.; Kolb, D. M. *Surf. Sci.* **1999**, *430*, L521−L526.
(22) Kolb, D. M. *Prog. Surf. Sci.* **1996**, *51*, 109−173.
(23) Kolb, D. M.; Dakkouri, A. S.; Batina, N. In *Nanoscale Probes of the Solid/Liquid Interface, NATO ASI Series*; Gewirth, A. A.; Siegenthaler, H. Eds.; Kluwer: Dordrecht, 1995; Vol. E288, p 263.
(24) Magnussen, O. M.; Hageböck, J.; Hotlos, J.; Behm, R. J. *Faraday Discuss.* **1992**, *94*, 329−338.
(25) Ye, S.; Ishibashi, C.; Uosaki, K. *Langmuir* **1999**, *15*, 807−812.
(26) Tremiliosi-Filho, G.; Dall'Antonia, L. H.; Jerkiewicz, G. *J. Electroanal. Chem.* **2005**, *578*, 1−8.
(27) Toney, M. F.; Melroy, O. R. Chapter 2 in *Electrochemical Interfaces: Modern Techniques for In Situ Interfacial Characterization*; Abruña, H. D. Ed.; VCH Publishers, Inc.: New York, 1991; p 55.
(28) Toney, M. F.; McBreen, J. *Interface*; The Electrochemical Society: Spring, 1993; Vol. 2, pp 22−31.
(29) de Moraes, I. R.; Nart, F. C. *J. Electroanal. Chem.* **1999**, *461*, 110−120.
(30) Horkans, J.; Cahan, B. D.; Yeager, E. *Surf. Sci.* **1974**, *46*, 1−23.
(31) Kolb, D. M. In *Spectroelectrochemistry, Theory and Practice*; Gale, R. J., Ed.; Plenum Press: New York, 1988; p 87.
(32) Kolb, D. M.; McIntyre, J. D. E. *Surf. Sci.* **1971**, *28*, 321−334.
(33) Friedrich, A.; Pettinger, B.; Kolb, D. M.; Lüpke, G.; Steinhoff, R.; Marowsky, G. *Chem. Phys. Lett.* **1989**, *163*, 123−128.
(34) Pettinger, B.; Lipkowski, J.; Mirwald, S.; Friedrich, A. *J. Electroanal. Chem.* **1992**, *329*, 377−382.
(35) Pettinger, B.; Lipkowski, J.; Mirwald, S. *Surf. Sci.* **1995**, *335*, 264−272.
(36) Yagi, I.; Chiba, M.; Uosaki, K. *J. Am. Chem. Soc.* **2005**, *127*, 12743−12746.
(37) Guyot-Sionnest, P.; Tadjeddine, A. *J. Chem. Phys.* **1990**, *92*, 734−738.
(38) Toney, M. F. in *Synchrotron Techniques in Interfacial Electrochemistry, NATO ASI Series*; Melendres, C. A.; Tadjeddine, A. Eds.; Kluwer Academic: Boston, 1994; p 109.
(39) Wang, J.; Ocko, B. M.; Davenport, A. J.; Isaacs, H. S. *Phys. Rev. B* **1992**, *46*, 10321−10338.
(40) Wang, J.; Davenport, A. J.; Isaacs, H. S.; Ocko, B. M. *Science* **1992**, *255*, 1416−1418.
(41) Ocko, B. M.; Wang, J. in *Synchrotron Techniques in Interfacial Electrochemistry, NATO ASI Series*; Melendres, C. A.; Tadjeddine, A. Eds.; Kluwer Academic: Boston, 1994; p 127.
(42) Ocko, B. M.; Wang, J.; Davenport, A.; Isaacs, H. S. *Phys. Rev. Lett.* **1990**, *65*, 1466−1469.
(43) Toney, M. F.; Gordon, J. G.; Sammant, M. G.; Borges, G. L.; Wiesler, D. G.; Yee, D.; Sorensen, L. B. *Langmuir* **1991**, *7*, 796−802.
(44) Toney, M. F.; Gordon, J. G.; Sammant, M. G.; Borges, G. L.; Melroy, O. R.; Yee, D.; Sorensen, L. B. *Phys. Rev. B* **1992**, *45*, 9362−9374.
(45) Scherb, G.; Kazimirov, A.; Zegenhagen, J.; Schultz, T.; Feidenhans'l, R.; Fimland, B. O. *Appl. Phys. Lett.* **1997**, *71*, 2990−2992.
(46) Takahasi, M.; Hayashi, Y.; Mizuki, J.; Tamura, K.; Kondo, T.; Naohara, H.; Uosaki, K. *Surf. Sci.* **2000**, *461*, 213−218.
(47) Uosaki, K.; Ye, S.; Kondo, T.; Naohara, H. In *Thin Solid Films: Preparation, Characterization, Applications*; Soriaga, M. P.; Stickney, J.; Bottomley, L. A.; Kim, Y.-G., Eds.; Kluwer Academic/Plenum Publishers: New York, 2002; pp 17−35.
(48) Kondo, T.; Tamura, K.; Takahasi, M.; Mizuki, J.; Uosaki, K. *Electrochim. Acta* **2002**, *47*, 3075−3080.
(49) Kondo, T.; Morita, J.; Okamura, M.; Saito, T.; Uosaki, K. *J. Electroanal. Chem.* **2002**, *532*, 201−205.
(50) Aruta, C.; Ricci, F.; Balestrino, G.; Lavanga, S.; Medaglia, P. G.; Orgiani, P.; Tebano, A.; Zegenhagen, J. *Phys. Rev. B* **2002**, *65*, 195408/1−195408/9.
(51) Tamura, K.; Wang, J.; Adzic, R. R.; Ocko, B. M. *J. Phys. Chem. B* **2004**, *108*, 1992−1998.
(52) Robinson, K. M.; Robinson, I. K.; O'Grady, W. E. *Surf. Sci.* **1992**, *262*, 387−394.
(53) Gibbs, D.; Ocko, B. M.; Zehner, D. M.; Mochrie, S. G. J. *Phys. Rev. B* **1988**, *38*, 7303−7310.
(54) Feidenhans'l, R. *Surf. Sci. Rep.* **1989**, *10*, 105−188.
(55) X-ray scattering by hydrogen atoms is so weak that we cannot determine the chemical nature of oxygen species, which can be an oxygen atom, OH, $OH^-$ ion, water molecule, $H_3O^+$, or sulfate anion, although sulfate anion can be distinguished by using the information for sulfur atoms.
(56) Ataka, K.; Osawa, M. *Langmuir* **1998**, *14*, 951−959.